


# 4D printing of biodegradable elastomers with tailorable thermal response at physiological temperature

**Journal Article****Author(s):**

Paunović, Nevena; Meyer, Daryl; Krivitsky, Adva; Studart, André R.; Bao, Yinyin; [Leroux, Jean-Christophe](#) 

**Publication date:**

2023-09

**Permanent link:**

<https://doi.org/10.3929/ethz-b-000627392>

**Rights / license:**

[Creative Commons Attribution 4.0 International](#)

**Originally published in:**

Journal of Controlled Release 361, <https://doi.org/10.1016/j.jconrel.2023.07.053>

**Funding acknowledgement:**

177178 - 3D printing manufacturing of patient-tailored drug releasing stents (SNF)



# 4D printing of biodegradable elastomers with tailorable thermal response at physiological temperature

N. Paunović<sup>a</sup>, D. Meyer<sup>a</sup>, A. Krivitsky<sup>a</sup>, A.R. Studart<sup>b</sup>, Y. Bao<sup>a,\*</sup>, J.-C. Leroux<sup>a,\*</sup>

<sup>a</sup> Institute of Pharmaceutical Sciences, Department of Chemistry and Applied Biosciences, ETH Zurich, 8093 Zurich, Switzerland

<sup>b</sup> Complex Materials, Department of Materials, ETH Zurich, 8093 Zurich, Switzerland

## ARTICLE INFO

**Keywords:**  
3D printing  
4D printing  
Shape-memory

## ABSTRACT

4D printing has a great potential for the manufacturing of soft robotics and medical devices. The alliance of digital light processing (DLP) 3D printing and novel shape-memory photopolymers allows for the fabrication of smart 4D-printed medical devices in high resolution and with tailorable functionalities. However, most of the reported 4D-printed materials are nondegradable, which limits their clinical applications. On the other hand, 4D printing of biodegradable shape-memory elastomers is highly challenging, especially when transition points close to physiological temperature and shape fixation under ambient conditions are required. Here, we report the 4D printing of biodegradable shape-memory elastomers with tailorable transition points covering physiological temperature, by using poly(D,L-lactide-co-trimethylene carbonate) methacrylates at various monomer feed ratios. After the programming step, the high-resolution DLP printed stents preserved their folded shape at room temperature, and showed efficient shape recovery at 37 °C. The materials were cytocompatible and readily degradable under physiological conditions. Furthermore, drug-loaded devices with tuneable release kinetics were realized by DLP-printing with resins containing polymers and levofloxacin or nintedanib. This study offers a new perspective for the development of next-generation 4D-printed medical devices.

## 1. Introduction

4D printing has attracted considerable interest since 2013, when it was first described in a scientific publication [1,2]. Initially, this terminology was used to refer to 3D printing processes with time as the fourth dimension [3,4]. However, in the last few years, 4D printing has evolved into a general concept that portrays stimuli-responsive 3D-printed objects, which change shape when triggered by heat, light, magnetic field or pH [3–7]. Among various materials for 4D printing, thermo-responsive shape-memory polymers (SMPs) represent one of the most promising classes [6,8,9], with potential for flexible electronics [10], soft robotics [11], and medical devices [12]. These 3D-printed materials can be deformed when heated above the transition point, and then fixed in a temporary shape when cooled below the transition temperature in a so-called programming step. When the objects are heated again above the transition point, they recover to their initial functional 3D-printed shape [5,6,9,10,13,14]. To apply SMPs in the clinic for e.g., 3D printing of intraluminal medical devices, the transition temperature (i.e., glass transition temperature or melting point) of the printed objects should ideally range between 37 and 41 °C to ensure

recovery of the device without the risk of thermal injury for the surrounding tissue [6,15–17].

Various additive manufacturing techniques have been used for SMP-based 4D printing, such as fused deposition modeling [11], direct ink writing [18], stereolithography (SLA) [19] and digital light processing (DLP) [20]. The latter two based on vat photopolymerization offer excellent printing resolution, shape fidelity and surface smoothness [21,22], which makes them superior to other rapid prototyping methods [23]. Following the pioneer work of Dunn [24] and Magdassi [10], a number of shape-memory devices have been manufactured by DLP/SLA [19,20,25–27] due to synthetic flexibility in the design of photopolymers. Despite the potential of 4D printing in the fabrication of personalized medical devices, most of the reported materials are rigid, nondegradable and exhibit shape recovery only at very high temperatures [24,28–30]. Although biodegradable and elastic SMPs have been widely reported [31–33], their 4D printing is still in its infancy [34].

Cohn and co-workers first reported 4D printing of a bioresorbable shape-memory personalized medical device [35]. They DLP printed a tracheal stent with a resin based on methacrylated poly( $\epsilon$ -caprolactone) (PCL) [35]. Recently, the same group extended the scope of their 4D-

\* Corresponding authors.

E-mail addresses: [ybao@ethz.ch](mailto:ybao@ethz.ch) (Y. Bao), [jleroux@ethz.ch](mailto:jleroux@ethz.ch) (J.-C. Leroux).

<https://doi.org/10.1016/j.jconrel.2023.07.053>

Received 14 February 2023; Received in revised form 13 July 2023; Accepted 30 July 2023

Available online 12 August 2023

0168-3659/© 2023 The Authors. Published by Elsevier B.V. This is an open access article under the CC BY license (<http://creativecommons.org/licenses/by/4.0/>).

printed materials to reach higher mechanical flexibility by adding a polypropylene glycol (PPG) block to the PCL photopolymers [12]. Although PCL-based SMPs can be successfully printed by vat photopolymerization, they are semicrystalline with transition temperatures usually higher than 50 °C, which places them out of the targeted range for biomedical applications. Even when the melting point can be decreased to physiological range by photopolymer engineering, as demonstrated in our previous work, the mechanical properties of the printed objects change dramatically above the transition temperature [34]. In parallel, Becker and co-workers developed a series of shape-memory poly(propylene fumarate) for 4D printing of bioresorbable complex scaffolds, which recover their functional shape at room temperature [36]. However, the medical application of such scaffolds would be impractical due to spontaneous recovery of the devices at the temperature of manipulation. Overall, it is highly challenging to 4D print biodegradable shape-memory elastomers with a transition point close to physiological temperatures and shape fixation under ambient conditions. If combined with the ability to release drugs in a controllable fashion, these two features would greatly contribute to the development of the next generation of 4D-printed medical devices.

Herein, we present the 4D printing of biodegradable shape-memory elastomers with tailorable transition points covering physiological temperatures by using poly(D,L-lactide-co-trimethylene carbonate) (poly(DLLA-co-TMC)) methacrylates with various monomer feed ratios (Fig. 1A). These materials displayed similar elasticity below and above their transition temperatures. The printing was performed via heat-

assisted DLP, which enabled the fabrication of highly elastic structures with high resolution and surface smoothness. After the programming step, the 4D-printed devices preserved their deformed shape at room temperature and showed efficient shape recovery at 37 °C. In addition, they were cytocompatible and readily degradable under physiological conditions. Moreover, 4D-printed shape-memory drug-eluting devices with tunable drug-release profiles were realized (Fig. 1B). This work demonstrates the practical potential of 4D-printed biodegradable elastomers for the next generation of multifunctional medical devices.

## 2. Materials and methods

### 2.1. Materials

3,6-Dimethyl-1,4-dioxane-2,5-dione (D,L-lactide, DLLA) was purchased from Sigma-Aldrich and Huizhou Foryou Medical Devices Co. Ltd. Trimethylene carbonate (TMC) was bought from Huizhou Foryou Medical Devices Co. Ltd. Methanol was obtained from VWR chemicals. Tetrahydrofuran (THF) was purchased from Merck Supelco and Acros Organics. Pentaerythritol, triethylamine (Et<sub>3</sub>N), Sudan I and THF (extra dry, over molecular sieve) were obtained from Acros Organics. Dimethylformamide (DMF) was obtained from Fisher Chemical. Levofloxacin was purchased from TCI. Nintedanib was provided by Ench Industry Co. Ltd. Phosphate buffered saline (PBS), Gibco Dulbecco's Modified Eagle Medium with high glucose, GlutaMAX™ supplement, pyruvate (DMEM), DMEM with high glucose, no glutamine, no phenol red (DMEM

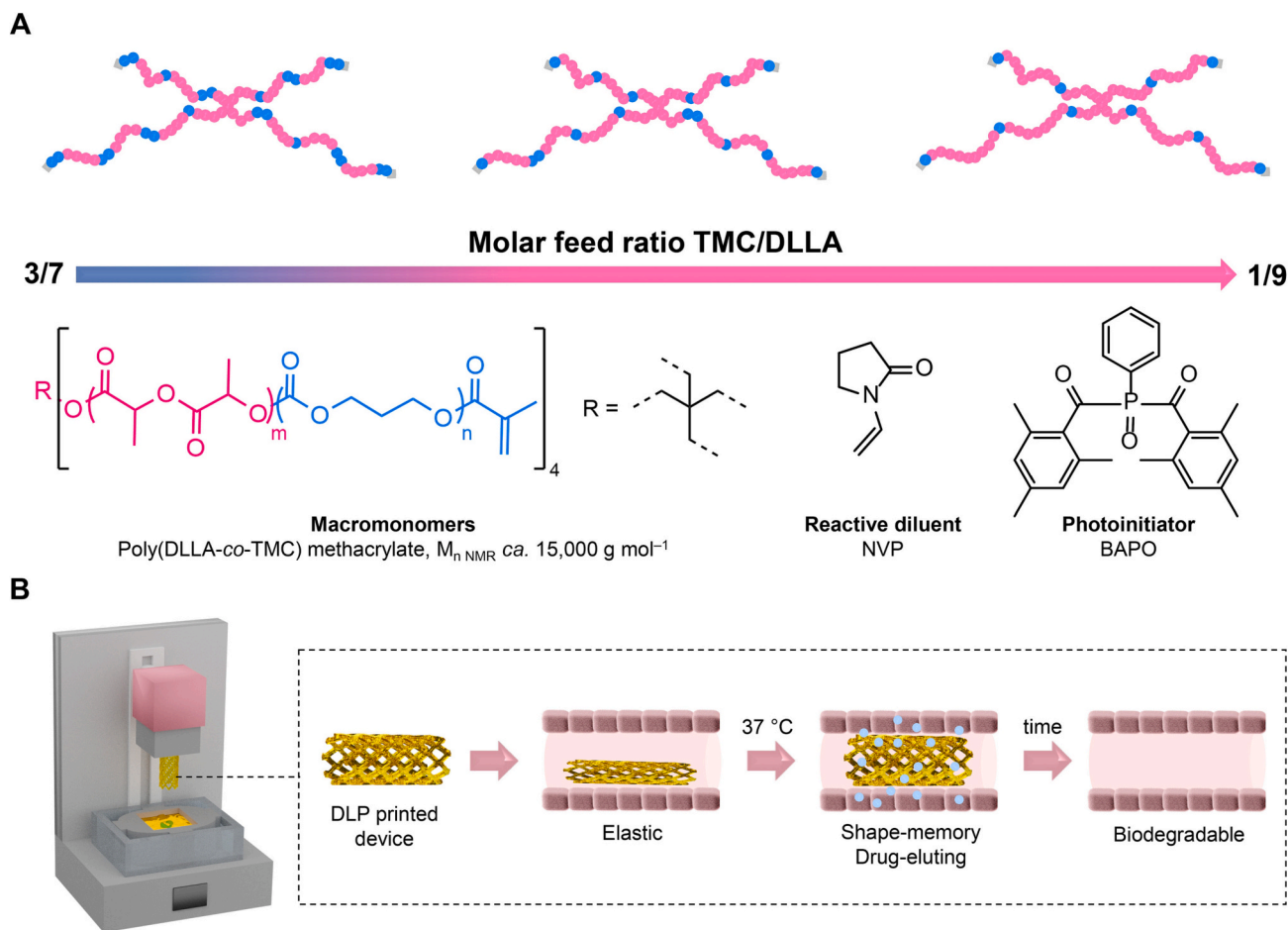


**Fig. 1.** 4D printing of biodegradable shape-memory elastomers with tailored transition temperature and tuneable drug release kinetics via DLP. (A) Design of novel biodegradable DLP-compatible resins based on poly(DLLA-co-TMC) methacrylates with various molar feed ratios of monomers for 4D printing. BAPO was used as a photoinitiator (1.0 wt%) and NVP as a reactive diluent (30 wt%). (B) Schematics of a 4D-printed elastic and biodegradable drug-eluting device with transition point at physiological temperature.

w/o dye), trypsin-EDTA (0.25%), fetal bovine serum (FBS) and penicillin/streptomycin solution were purchased from Thermo Fisher Scientific. Cell titer 96® Aqueous One Solution Proliferation Assay (MTS) was bought from Promega AG. All other chemicals were obtained from Sigma-Aldrich. All chemicals were used as purchased.

## 2.2. Polymer synthesis

Poly(DLLA-co-TMC)s were synthesized by ring-opening polymerization of TMC and DLLA in melt initiated by pentaerythritol, with tin(II)-2-ethylhexanoate ( $\text{Sn}(\text{Oct})_2$ ) as a catalyst (Fig. S1) [37]. Statistical copolymers with MW of  $\sim 15,000 \text{ g mol}^{-1}$  and different molar feed ratios of monomers (TMC: DLLA 7:3, 5:5, 3:7, 2:8 and 1:9) were prepared. Representative synthesis of poly(DLLA-co-TMC) with 70 mol% of DLLA: pentaerythritol (0.18 g, 1.33 mmol), DLLA (15.13 g, 105 mmol), TMC (4.61 g, 45.2 mmol) and  $\text{Sn}(\text{Oct})_2$  (4  $\mu\text{L}$ , 0.013 mmol) were added to a Schlenk flask and placed under vacuum for 1.5 h to eliminate oxygen and water. The flask was then purged with argon, placed in an oil bath at 140 °C and stirred for 24 h. The obtained polymer was dissolved in THF and precipitated in hexane. Based on  $^1\text{H}$  nuclear magnetic resonance ( $^1\text{H}$  NMR) spectroscopy, the conversions of DLLA and TMC for all synthesized copolymers were ca. 97–99 and 86–98%, respectively (Fig. S2). Poly(DLLA-co-TMC) was further dissolved in extra dry THF (100 mL),  $\text{Et}_3\text{N}$  was added (2.8 mL, 20.0 mmol) and the solution was purged with argon for 15 min. Methacryloyl chloride (1.9 mL, 20.0 mmol) was then mixed with extra dry THF (5 mL) and added dropwise to the polymer solution. The reaction was stirred under argon at room temperature for ca. 12 h [38,39]. Afterwards, the reaction mixture was centrifuged (3500  $\times$ g, 4 °C, 20 min) in order to remove salts, and (+)- $\alpha$ -tocopherol was added to the supernatant (0.15 g). After purification in methanol, the conversion of terminal hydroxyl groups was determined to be ca. 85–100%, except for 50 mol% DLLA photopolymer with 59% (Fig. S3) based on  $^1\text{H}$  NMR. Polydispersity of resulting copolymers was determined by size exclusion chromatography (SEC) (Table S1).

## 2.3. Characterization of polymers

$^1\text{H}$  NMR spectra were recorded on Bruker AV400 spectrometer at 400 Hz using  $\text{CDCl}_3$  as a solvent. SEC was accomplished by using a Viscotek TDAmx system equipped with two Viscotek columns (D3000, poly(styrene-co-divinylbenzene)) at 40 °C and differential refractive index detector (TDA 302, Viscotek). All samples were dissolved in DMF with LiBr (0.1 wt%), filtered through 0.2  $\mu\text{m}$  syringe filters (polytetrafluoroethylene, PTFE) and eluted by DMF with LiBr (0.1 wt%) as a mobile phase at 0.5 mL  $\text{min}^{-1}$  flow rate. The molecular weights and polydispersity indexes were determined relative to a poly(methyl methacrylate) (PMMA) standard curve (PSS polymer Mainz, 2500–89,300  $\text{g mol}^{-1}$ ) by using OmniSEC software (v5.0, Malvern Panalytical). Differential scanning calorimetry (DSC) analysis was performed by TA Q200 DSC (TA Instruments–Waters LLC). The samples (ca. 10 mg) in Tzero hermetic pans (TA Instruments–Waters LLC) were exposed to heat-cool-heat cycles from room temperature to 200 or 250 °C in the first and from –60 to 100 or 250 °C in the second heating cycle under nitrogen flow (50 mL  $\text{min}^{-1}$ ) with heating and cooling rates of 10 °C  $\text{min}^{-1}$ . Data were analysed with the TA Instruments Universal Analysis 2000 software (5.5.3). Viscosity was determined at a shear rate of 100  $\text{s}^{-1}$  in the temperature range of 75 to 95 °C or 80 to 100 °C, by applying a heating rate of 0.05 °C  $\text{s}^{-1}$  on a HAAKE RheoStress 600 rotational rheometer (Thermo Electron Corporation) equipped with cone and plate geometry (35  $\text{mm}^2$ ). Data were analysed by RheoWin Data Manager (Thermo Electron Corporation). Fourier transform infrared (FTIR) spectra were recorded on a Perkin-Elmer Spectrum 65 (Perkin-Elmer Corporation) in transmission mode in the range of 650 to 4000  $\text{cm}^{-1}$ .

## 2.4. DLP printing

Biomedical inks were prepared by melting photopolymers in the presence of an antioxidant ((+)- $\alpha$ -tocopherol, 0.3 wt%) and mixing them with a solution of photoinitiator phenylbis(2,4,6-trimethyl-benzoyl) phosphine oxide (BAPO, 1.0 wt%) and the photoabsorber (Sudan I, 0.03 wt%) in a reactive diluent N-vinylpyrrolidone (NVP, 30 wt%). In case of drug-containing inks, levofloxacin or nintedanib (1 wt%) were also dissolved in NVP. The inks were further sonicated at 80 °C until they became homogenous. All objects were printed on heat-assisted DLP 3D printer (Asiga PICO2) with the light source of 405 nm [38]. The printing temperature was set to 85–90 °C, while exposure time and initial exposure time were 3.3 and 15–30 s, respectively. Drug-eluting materials were printed with exposure times of 5 and 10 s, while initial exposure times were 10 and 15 s, for levofloxacin and nintedanib sets, respectively. The control materials were printed with exposure time and initial exposure time of 5 and 10 s, respectively. Afterwards, the printed objects were washed in acetone and 2-propanol and then cured in an Asiga Pico Flash UV chamber for 30 min.

## 2.5. Mechanical characterization of 3D-printed objects

Tensile tests at room temperature were performed on an AGS-X (Shimadzu) universal testing machine with a 100-N load cell at a rate of 20  $\text{mm min}^{-1}$  and a gauge length of 13 mm using dog-bone specimens. Tensile tests at 37 °C with their corresponding controls at room temperature were conducted on Instron 5500 with integrated environmental chamber and a 100-N load cell, at a crosshead speed of 11  $\text{mm min}^{-1}$ . Data were analysed with Bluehill 2 software (Instron). Drug-containing and their control bare-polymer dog-bone-shaped specimens were programmed (heating to 80 °C and then cooling to –20 °C with 10 min for each step) and tested at room temperature at a crosshead speed of 0.10  $\text{mm s}^{-1}$  on TA.XT plus texture analyzer (Stable Micro Systems) with ca. 500-N load cell. Engineering stress ( $\sigma$ ) and strain ( $\epsilon$ ) were calculated using Eqs. 1 and 2, respectively [40]

$$\sigma = \frac{F}{A_0} \quad (1)$$

$$\epsilon = \frac{L}{L_0} \times 100 \quad (2)$$

where  $F$  is the force,  $A_0$  is the initial cross-sectional area (ca. 1.5  $\text{mm}^2$ ),  $L$  is the elongation, and  $L_0$  is the initial gauge length (ca. 11–13 mm). Young's modulus was calculated as a slope of the initial linear region (first 10 points for ASG-X and TA.XT plus, first 160 points for Instron 5500) of tensile stress-strain curves.

## 2.6. Microscopy

3D-printed objects of complex architectures and dog-bone-shaped specimens after 1 week treatment in water or PBS were visualized using a Keyence scanning laser microscope (Keyence Corporation).

## 2.7. Shape memory properties

Poly(DLLA-co-TMC) methacrylate-based cuboids (12.5  $\times$  2.4  $\times$  0.8 mm) with 70, 80 and 90 mol% DLLA were evaluated for their shape-memory properties ( $\theta_{\text{max}}$ ). Each sample was first heated to 80 °C for 2 min and then deformed and placed in a 200- $\mu\text{L}$  pipette tip. Further, the samples were kept at –20 °C for 10 min and the maximal angle ( $\theta_{\text{max}}$ ) was recorded by a phone camera. Then, the external force was removed and the sample was left at –20 °C for 2 min, which was referred as a fixed angle ( $\theta_{\text{fixed}-20}$ ). Another fixed angle ( $\theta_{\text{fixed RT}}$ ) was captured after additional 2 min at room temperature. Then, the samples were placed in an oven at 37 °C for 5 min and the unrecovered angle ( $\theta_{\text{unrecovered}}$ ) was recorded [41]. Shape fixity ratio at –20 °C ( $R_{f-20}$ )

and at room temperature ( $R_{f\ RT}$ ), as well as shape recovery ratio ( $R_r$ ) were calculated using Eqs. 3, 4 and 5, respectively:

$$R_{f\ -20\ ^\circ\text{C}} = \frac{\theta_{\text{fixed}\ -20\ ^\circ\text{C}}}{\theta_{\text{max}}} \times 100 \quad (3)$$

$$R_{f\ RT} = \frac{\theta_{\text{fixed}\ RT}}{\theta_{\text{max}}} \times 100 \quad (4)$$

$$R_r = \frac{\theta_{\text{max}} - (\theta_{\text{unrecovered}} - \theta_0)}{\theta_{\text{max}}} \times 100 \quad (5)$$

## 2.8. Degradation study

Four stent-like prototypes (H 10.0 mm,  $\varnothing$  7.2 mm, thickness 1.0 mm) were DLP printed with 70, 80 and 90 mol% DLLA photopolymers. They were programmed (heating with a heating gun and cooling to  $-20\ ^\circ\text{C}$  for 10 min) and placed separately in closed Falcon® tubes with 50 mL PBS pH 7.4 at  $37\ ^\circ\text{C}$ . At each time point, the specimens were taken out, rinsed with deionized water, wiped with paper tissue and dried under vacuum at  $50\ ^\circ\text{C}$  for  $24 \pm 1$  h. At the same time, the buffer was replaced with a fresh one. The water uptake (wt%) was calculated according to Eq. 6

$$\text{water uptake} = \frac{w_{\text{wet}} - w_{\text{dry}}}{w_{\text{dry}}} \times 100 \quad (6)$$

where  $w_{\text{wet}}$  is the mass of a tubular object in a wet state after the wiping with a paper tissue and  $w_{\text{dry}}$  is the mass of a stent in a dry state after drying under vacuum. One stent with 80 mol% DLLA lost its structure at week 8, while at week 10 all stents collapsed after drying.

Uniaxial compression tests were performed on stents in wet states using TA.XTplus texture analyzer (Stable Micro Systems) with ca. 500-N load cell at the compression rate of  $12\ \text{mm}\ \text{min}^{-1}$ . During first two weeks all stents were compressed to ca. 60% of their inner diameter. The distance was then decreased to 15% and only materials with 70 and 80 mol % DLLA were compressed for two more weeks.

## 2.9. Cell culture

Human cervical epithelial cells (HeLa, ATCC) were used up to passage number 11 and were tested for mycoplasma contamination (MycoAlert™ Mycoplasma Detection Kit, Lonza) at first and last passage number. They were cultured in complete medium DMEM (high glucose, GlutaMax™, pyruvate) with 10% fetal bovine serum and 1% penicillin-streptomycin at  $37\ ^\circ\text{C}$  in a humidified atmosphere with 5%  $\text{CO}_2$ .

## 2.10. In vitro cytocompatibility test

The cytotoxicity tests were conducted in 24-well plates with 40,000 cells per well in three independent experiments with three replicates. For positive control, cells were incubated in complete medium with 100 mM hydrogen peroxide, while for negative control, complete medium only was used. All 3D-printed disks (H 0.8 mm,  $\varnothing$  5.5 mm) were thoroughly cleaned [38], placed on Transwell® permeable supports (Thin-Cert™ Cell Culture Inserts 24-well, sterile, translucent, pore size 8  $\mu\text{m}$ ; Greiner Bio-One) and inserted above the seeded cells. Medium (100  $\mu\text{L}$ ) was added on the top of the inserts and the plate was incubated for  $48 \pm 1$  h. Cell viability was calculated based on the absorbance measured in the 3-(4,5-dimethylthiazol-2-yl)-5-(3-carboxymethoxyphenyl)-2-(4-sulphophenyl)-2H-tetrazolium (MTS) assay (CellTiter 96® Aqueous One Solution Cell Proliferation Assay, G3580; Promega) as a percentage of the negative control.

## 2.11. In vitro drug release

3D-printed cuboids ( $25 \times 10 \times 1$  mm) based on poly(DLLA-co-TMC)

methacrylates with 70 or 90 mol% DLLA and 1 wt% of levofloxacin or nintedanib were programmed (heating to  $80\ ^\circ\text{C}$  and then cooling to  $-20\ ^\circ\text{C}$  with 10 min for each step) and then placed separately into closed containers with 50 mL PBS pH 7.4 at  $37\ ^\circ\text{C}$ . A sample (10 mL) was taken from each tube (four samples per composition) every day for 3 days and then every 3–4 days. At each time point, complete medium was replaced with fresh PBS pH 7.4 to ensure sink conditions. All samples were freeze-dried and then each one was dissolved in a 1-mL of mobile phase A (1% TEA solution, adjusted to pH 2.5 with phosphoric acid). Mobile phase B was acetonitrile. The samples (50  $\mu\text{L}$ ) were injected in Chromaster HPLC equipped with diode array detector (VWR Hitachi) and XBridge C18 5  $\mu\text{m}$  column (Waters). A gradient elution was performed with the mixture of mobile phases A and B (14–25% of mobile phase B over 10 min for levofloxacin and 30–40% over 11 min for nintedanib) at a flow rate of  $1\ \text{mL}\ \text{min}^{-1}$ . The drug content was determined at 295 and 395 nm for levofloxacin and nintedanib, respectively. The limit of quantification (LoQ) was 0.0025 mg  $\text{mL}^{-1}$  for levofloxacin and 0.000391 mg  $\text{mL}^{-1}$  for nintedanib. Levofloxacin samples which were below the LoQ were analysed using fluorescence detector, with excitation wavelength of 295 nm and emission wavelength of 490 nm [42]. Calibration curves were run in triplicates using a serial dilutions of stock solutions (0.15 mg  $\text{mL}^{-1}$  in mobile phase A). Linear regression line was fitted with the use of least squares. The correlation coefficient was above 0.99.

## 2.12. Statistical significance

Statistical significance was assessed by one-way ANOVA with Tukey's comparison test with  $p$ -value  $< 0.05$  considered significant using OriginPro 2019 (OriginLab Corporation).

## 3. Results and discussion

### 3.1. Design and characterization of novel biodegradable inks for 4D printing

We recently described the DLP 3D printing of biodegradable elastic medical devices, such as non-vascular stents [38,43,44]. However, these systems were lacking intrinsic shape-memory properties that would allow them to be deployed in a deformed shape and then spontaneously self-open at physiological temperature. In order to produce such multifunctional medical devices, a series of biodegradable poly(DLLA-co-TMC)s was synthesized by ring opening polymerization of DLLA and TMC at different molar feed ratios (Figs. 1A and S1). The copolymers were further methacrylated at terminal ends to introduce crosslinkable moieties (Fig. S1). The molecular weight (MW) was kept constant at ca. 15,000 g  $\text{mol}^{-1}$  (Table S1) to provide elasticity.

While the use of high MW macromonomers is essential for elasticity and degradability, it makes the resins highly viscous and thus difficult to be printed into high-resolution objects [34,45–47]. Hence, we selected statistical copolymers, which are known to be less viscous than the homopolymers of the same MW [39,48,49]. A four-arm structure was also employed to further reduce the viscosity. Still, the synthesized macromonomers were too viscous for DLP printing at room temperature. Therefore, we included NVP (30 wt%) as a reactive diluent (Fig. 1A) to reduce the viscosity of most resins to a printable range at  $80\ ^\circ\text{C}$  (Fig. 2A). Moreover, NVP was used to dissolve the photoinitiator BAPO (1 wt%, Fig. 1A) and the photoabsorber Sudan I (0.03 wt%). Antioxidant (+)- $\alpha$ -tocopherol was also added to the formulation to prevent premature crosslinking of the photopolymers.

### 3.2. Thermal and mechanical properties of DLP-printed biodegradable elastomers

All resins were printed at  $80$ – $90\ ^\circ\text{C}$  by heat-assisted DLP [34,38,43,44]. The glass transition temperature ( $T_g$ ) of the printed samples gradually shifted from ca.  $-14$  to  $42\ ^\circ\text{C}$  when the amount of



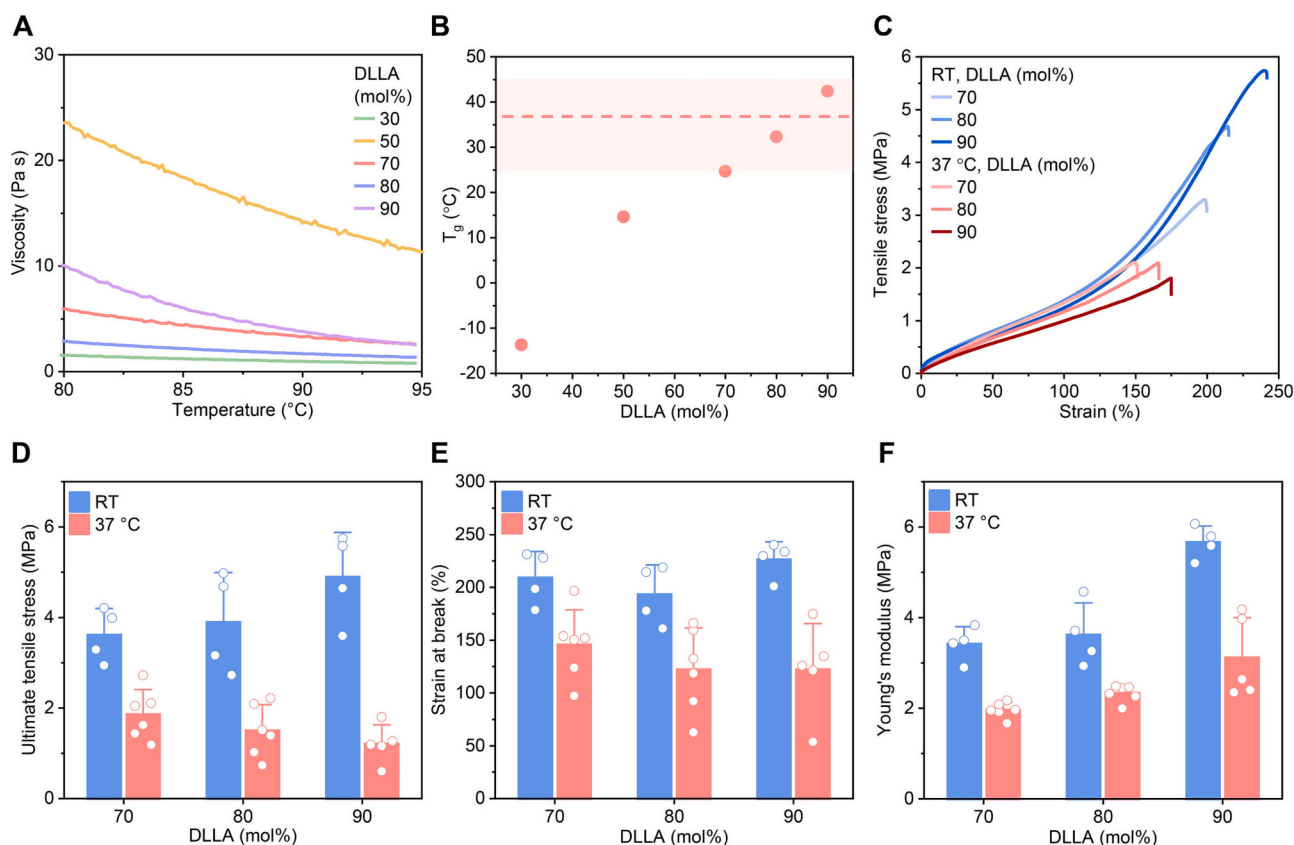


**Fig. 2.** Thermal and mechanical properties of DLP printed biodegradable elastomers based on poly(DLLA-co-TMC) methacrylates with different molar feed ratios of DLLA. (A) Viscosity of resins with 30 wt% of NVP. (B) Dependence of the transition point on molar feed of DLLA. (C) Representative engineering stress-strain curves obtained with dog bone-shaped specimens in a tensile test performed at room temperature and at 37 °C. (D-F) Average ultimate tensile stress (D), strain at break (E) and Young's modulus (F) of DLP printed dog-bone shaped specimens at room temperature and at 37 °C. Mean + s.d. ( $n = 4-6$ ).

DLLA was increased from 30 to 90 mol% (Figs. 2B and S4). This is in line with the  $T_g$  of their respective macromonomers ranging from  $-15$  to  $29$  °C (Fig. S4), which fell between the reported  $T_g$  of PDLLA (ca.  $54$  °C) [50] and PTMC (ca.  $-14$  °C) [51,52]. It should be noted that the printing process was straightforward for all the investigated resins, except for the formulation based on a copolymer with an equimolar ratio of monomers, which was more challenging to print due to its high viscosity (Fig. 2A).

The  $T_g$  of 3D-printed poly(DLLA-co-TMC) methacrylates with 70, 80, and 90 mol% DLLA was 25, 32 and 42 °C, respectively, which might enable their shape recovery close to physiological temperature. Complete crosslinking of vinyl groups in the 3D-printed materials was observed by FTIR (Fig. S5), indicating a minimal safety risk related to the residual NVP [53] and methacrylate groups [54], while in the case of further development, the residual amount of NVP would have to be precisely quantified in order to meet regulatory requirements. Thus, these materials were selected for further mechanical and 4D printing evaluation.

All three resin formulations allowed for 3D printing of hyperelastic materials (Fig. 2C), with greater strength and stretchability at room temperature (ca.  $22$  °C) compared to that at 37 °C. This is explained by the higher chain mobility above or close to the transition point. At room temperature, the average ultimate tensile stress increased from 3.6 to 4.9 MPa when DLLA content was raised from 70 to 90 mol% (Fig. 2D), while the elongation at break was similar with values ranging from ca. 200 to 230% (Fig. 2E). All materials were highly elastic, with Young's modulus between 3.5 and 5.7 MPa, corresponding to DLLA content ranging from 70 to 90 mol% (Fig. 2F).

At the physiological temperature, the ultimate tensile stress decreased to 1.2–1.9 MPa (Fig. 2D) and strain at break to 120–145% (Fig. 2E), while the differences between the materials became even

lower. The average Young's modulus was not substantially affected (2.0–3.1 MPa), with materials containing 80 and 90 mol% DLLA showing lower elasticity (Fig. 2F). It should be noted that the difference in Young's modulus of the printed elastomers below and above the  $T_g$  was much smaller than that of previously reported 4D-printed SMPs such as PCL [10].

Overall, the monomer feed ratio of photopolymers can be changed to successfully 3D print biodegradable elastomers with tailorable  $T_g$  covering physiological temperature, while maintaining similarly high elasticity below and above the transition point.

### 3.3. 4D printing and shape-memory properties

To demonstrate that high-resolution devices could be produced with the developed resins, we printed honeycomb structures with cell thickness of ca.  $350$   $\mu\text{m}$  based on all three selected photopolymers (Fig. 3A). As shown in Fig. 3B, the highly elastic 3D-printed objects had smooth surfaces and could be easily folded like a silicone rubber.

Subsequently, we tested the suitability of resins for 4D printing of elastomers by fabricating a simple ETH logo structure using the 90 mol% DLLA photopolymer. The object was heated with a heating gun, deformed and rapidly cooled down in a programming step. Thanks to the shape-memory properties, fast and efficient shape recovery above its transition point was achieved (Fig. 3C). For a medical application, the programming step can be performed by heating the stent at  $50$  °C, folding it and then fixing it at  $-20$  °C, while the recovery occurs at body temperature (Fig. 3D). We validated the proposed protocol with meshed stents in human size (H 25 mm and  $\varnothing$  10.8 mm) which were DLP printed with all three selected resins (Fig. 3E). As expected, the stent based on poly(DLLA-co-TMC) with 70 mol% of DLLA showed the fastest shape

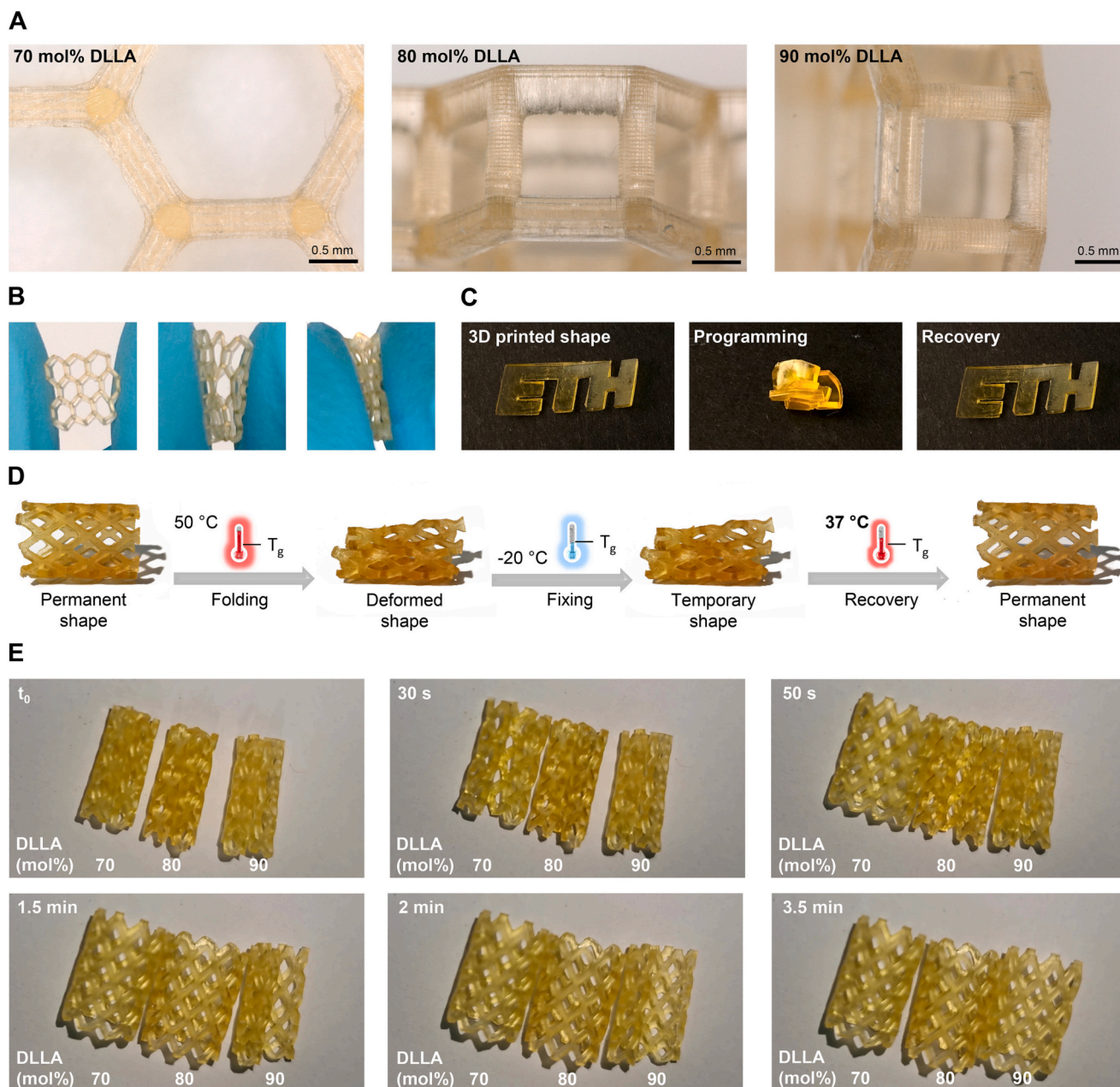


**Fig. 3.** 4D printing and shape-memory properties of biodegradable elastomers based on poly(DLLA-co-TMC) methacrylates. (A) Microscopy images of DLP printed objects based on 70, 80 and 90 mol% DLLA photopolymers, from the left to the right, showing high resolution. (B) Elasticity of the printed objects illustrated by finger compression of a sample based on 80 mol% DLLA photopolymer. (C) Shape recovery of 4D-printed ETH logo based on 90 mol% DLLA photopolymer initiated by a heating gun following the programming step. (D) Protocol for facilitated insertion of 4D-printed stents, including programming step (folding at temperature above  $T_g$  and freezing to temperature below  $T_g$ ) with 80 mol% DLLA elastomer as an example. (E) Self-opening of 4D-printed stents (H 25 mm and  $\varnothing$  10.8 mm) based on 70, 80, and 90 mol% DLLA photopolymers at 37 °C after the programming step.

recovery at 37 °C by fully opening within 50 s. The stent with 80 mol% of DLLA needed 1.5 min to fully recover, while the 90 mol% DLLA stent recovered its functional shape after 3.5 min. Furthermore, all elastomers maintained good shape fixity not only at -20 °C (ca. 100%, Fig. S6 and Table S2) but also at room temperature (89–98%, Fig. S6 and Table S2), indicating the potential of these 4D-printed devices to be shortly manipulated under ambient conditions before the insertion. All materials exhibited good shape recovery from 97 to 100% at 37 °C (Fig. S6 and Table S2).

### 3.4. Biodegradability

The biodegradability of these shape-memory elastomers was further

investigated on DLP printed tubular objects incubated in PBS pH 7.4 at 37 °C. As shown in Fig. 4A, all three materials demonstrated similar degradation profiles under physiological conditions. Autocatalytic bulk degradation was identified as the degradation mode [55], with low weight loss (< 10 wt%) during the first 6 weeks followed by rapid degradation. This resulted in massive weight loss (ca. 50 wt%) and structural collapse of most of the samples at week 10. Some samples already fragmented at week 8, causing large fluctuations in reported weight losses. The observed degradation behaviour was typical of polyester-based materials [56]. It is related to accumulation of acidic monomers and oligomers inside the polymer network, which accelerate the hydrolysis [39,55,57], while the surface degrades slowly, due to buffering capacity of the surrounding medium [58,59]. The trend



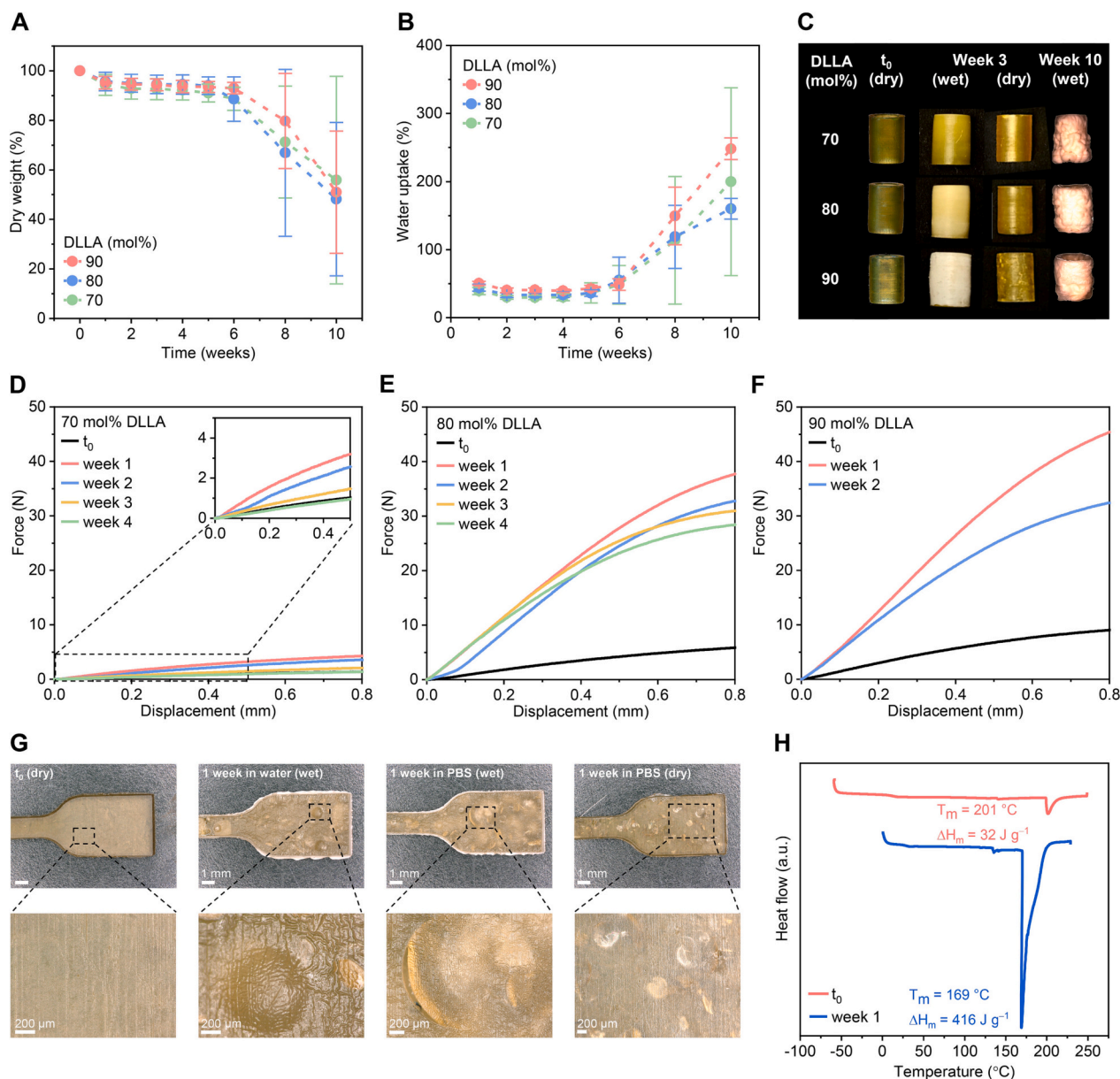


**Fig. 4.** Degradation behaviour of 4D-printed shape-memory elastomers based on poly(DLLA-co-TMC) methacrylates. (A and B) Weight loss (A) and water uptake (B) of printed tubular objects (H 10.0 mm,  $\varnothing$  8.0 mm, thickness 1.0 mm) over time in PBS pH 7.4 at 37 °C. Mean  $\pm$  s.d. ( $n = 4$ ). (C) Photographs of representative stents at the beginning of the degradation study ( $t_0$ ) in a dry state, after 3 weeks in wet and dry states, and after 10 weeks in a wet state, from the left to the right. (D to F) Compression curves of a representative stent in a wet state based on 70 (D), 80 (E) and 90 mol% (F) DLLA photopolymers during degradation. Inset (D): force-displacement curves at low displacement (up to 0.5 mm). (G) 3D-printed dog-bone-shaped specimen based on 80 mol% DLLA photopolymer in a dry state, after a week in water in a wet state, and after a week in PBS in both wet and dry states, from the left to the right. (H) DSC curves from the first heating cycles of materials based on 80 mol% DLLA photopolymer after 3D printing and after a week in PBS.  $T_m$  and  $\Delta H_m$  are indicated on the graph.

observed in weight loss positively correlates with water uptake, with 30–40 wt% gain during the first 6 weeks (Fig. 4B), and 150–250 wt% at the time of the structural collapse (i.e., at week 10). Less hydrophobic polymer networks, with higher content of DLLA were characterized by higher water uptake (Fig. 4B), which was also visually observed at week 3 (Fig. 4C). Toward the end of the degradation process, bubble-like structures could be observed in wet stents that remained intact at week 10 (Fig. 4C). This could be explained by big voids that are created after the release of degradation products from the inner parts of the crosslinked network [60,61].

A particularly interesting phenomenon was observed when following the mechanical properties of the stents in a wet state, which is clinically relevant, during the degradation study. All stents became much stiffer after the first week of degradation (Fig. 4D to F), which

could probably be related to the initial weight loss of ca. 5 wt%. The formed cavities might have enabled the reorganization of lactide-dominant polymer chains allowing them to crystallize [60,61]. This hypothesis is in accordance with the stiffening effect that was more pronounced for the materials based on 80 and 90 mol% DLLA photopolymers (Fig. 4E and F), while the sample containing 70 mol% DLLA photopolymer remained elastic (Fig. 4D). In the following weeks, the stents displayed a gradual decrease in resistance to uniaxial compression (Fig. 4D to F). Stent prototypes with 90 mol% DLLA needed to be excluded from the compression study after 2 weeks, due to their remarkably high stiffness (Fig. 4F). Indeed, the wet stents with higher amount of DLLA were more opaque (Fig. 4C) indicating larger crystal phases and a higher degree of crystallinity [62].

To further investigate the stiffening effect, 3D-printed dog-bone-



shaped specimens were incubated in water or PBS at 37 °C. By optical microscopy, we identified structural rearrangement with big voids and crystals (Fig. 4G). The  $T_m$  decreased, due to the presence of water [61,62], while  $\Delta H_m$  increased after a week of degradation, indicating higher degree of crystallinity (Fig. 4H) [61]. Furthermore, the effect of salts in the wet state could be excluded, as there was no statistically significant difference between mechanical properties of samples incubated in water or PBS (Fig. S7). After drying, the samples became even stronger and stiffer, which correlates to the crystalline domains identified in microscopy images (Fig. 4G). Thus, the stiffening effect could probably be attributed to the initial degradation in the aqueous environment and the creation of voids inside the polymer network, which facilitated polymer chain rearrangement leading to crystallization. Depending on the application, this effect may cause irritation and discomfort, as the pressure exerted by the stent may be too high for the surrounding tissue. On the other hand, the low extent of stiffening over time could also be beneficial, as it may ensure better positioning of the stent, which would, otherwise, lose its strength, resulting in migration. Furthermore, these materials may find their use in applications other than stenting [63] where self-stiffening is desired. The possibility to program the extent of this effect should be further evaluated in a more systematic study.

### 3.5. Cytocompatibility and drug release

With excellent mechanical performance, shape-memory properties and biodegradability obtained, we further evaluated the cytocompatibility of these 4D-printed elastomers. DLP samples printed with 70, 80 and 90 mol% DLLA photopolymers were placed in Transwell® supports and incubated with HeLa cells for  $48 \pm 1$  h. Cell viability was estimated based on MTS assay, with values obtained from cells incubated with medium only as a reference. All tested materials showed no significant influence on cell viability when compared to the medium control (Fig. 5A).

Furthermore, to demonstrate the suitability of these novel 4D-printed biodegradable elastomers for manufacturing of drug-eluting devices, poly(DLLA-co-TMC) methacrylates with 70 or 90 mol% of DLLA were physically mixed with 1 wt% of levofloxacin or nintedanib and then printed by DLP. Levofloxacin and nintedanib were selected as two chemically distinct drugs (Fig. 5B) with roles in treating bacterial infections and fibrosis, respectively. All four formulations exhibited sustained release over a month of incubation in PBS pH 7.4 at 37 °C (Fig. 5C). Levofloxacin-eluting devices showed burst and much higher relative release (15–23%) than nintedanib ones (1–3%) due to the higher water solubility of levofloxacin (*ca.* 17 mg mL<sup>-1</sup>) [64] over

nintedanib (5 µg mL<sup>-1</sup>) [65]. The release kinetics could also be manipulated by tuning the polymer composition. The less hydrophobic polymer network with 90 mol% of DLLA was associated with the higher burst and total release of levofloxacin, which could result from the higher water uptake (Fig. 4B) that promoted the dissolution and diffusion of the drug. Even at the point of the structural collapse of the elastomers (Fig. 4A), the drug release kinetics was not affected, indicating that drug molecules stayed entrapped in the remaining soft pieces. In the case of medical devices, such as airway stents, antibiotics are given shortly after the insertion to prevent infections related to the procedure itself [66]. Therefore, a rapid release of levofloxacin following the insertion procedure would be desirable in a clinical setting. On the other hand, devices with antifibrotic agents should rather be designed with a low sustained release due to delayed onset of fibrosis [67]. Thus, the observed release profiles are expected to be suitable from a clinical perspective.

The drug incorporation strengthened the elastomers and made them stiffer, independently of the drug type, while the elongation at break was only slightly affected (Fig. S8). While the drug loading of the materials developed in this study is already much higher than in conventional surface-coated drug-eluting medical devices [68], the changes in mechanical properties of the elastomer could be more prominent if higher amounts of drugs are needed. Therefore, the stiffening effect achieved in the presence of drugs should be taken into account when designing devices for a specific application.

## 4. Conclusions

We developed DLP printed thermally-responsive elastomers based on methacrylated poly(DLLA-co-TMC) photopolymers with tunable transition points around physiological temperature. The materials became only slightly more elastic at 37 °C when compared to room temperature, as opposed to previously reported systems. 4D-printed stents with 70, 80 and 90 mol% DLLA photopolymers showed good shape fixity at room temperature with shape recovery at 37 °C within 3.5 min, making them suitable candidates for biomedical applications. Furthermore, the printed elastomers were cytocompatible and degraded under physiological conditions over 2.5 months, which further corroborate their potential for the manufacturing of shape-memory medical devices. Drug-eluting devices based on these 4D elastomers displayed sustained drug release that could be modulated by changing the photopolymer composition. The reported elastic, shape-memory and biodegradable materials with the capacity for drug incorporation, could accelerate the translation of 4D printing research toward the on-demand fabrication of personalized multifunctional devices, such as non-vascular stents.

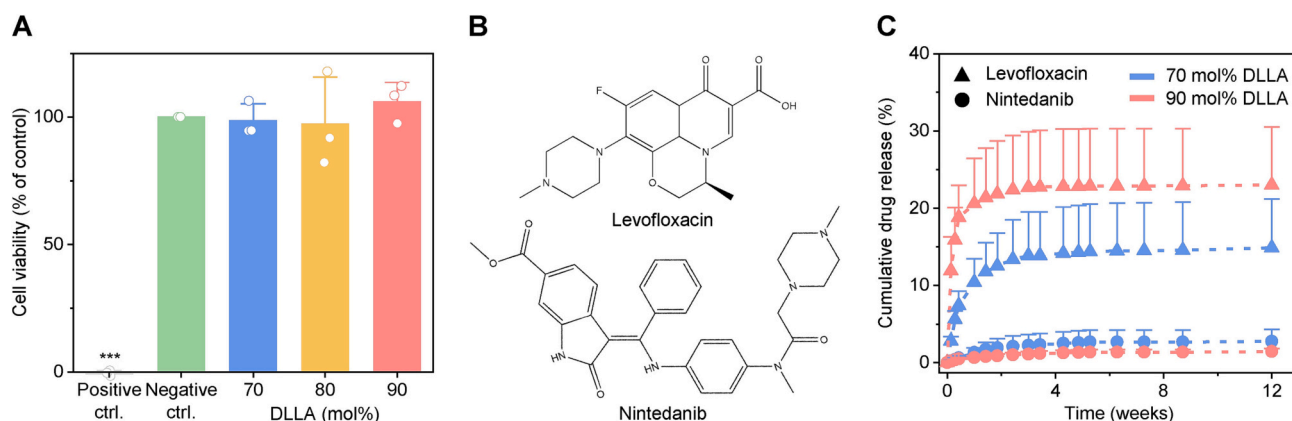


**Fig. 5.** Cytocompatibility of 4D-printed elastomers and drug release profiles of drug-eluting devices with 1 wt% of levofloxacin or nintedanib. (A) Cell viability after incubation with DLP printed materials compared to medium control (green bar) based on MTS assay. Positive control (100 mM hydrogen peroxide) corresponds to the first column. Mean + s.d. ( $n = 3$ ). Statistical significance was calculated by one-way ANOVA with Tukey's comparison test with  $***p < 0.001$ . (B) Chemical structures of levofloxacin and nintedanib. (C) Drug release profiles from DLP printed cuboids ( $25 \times 10 \times 1$  mm) in PBS pH 7.4 at 37 °C. Mean + s.d. ( $n = 4$ ).

Supplementary data to this article can be found online at <https://doi.org/10.1016/j.jconrel.2023.07.053>.

### CRediT authorship contribution statement

**N. Paunović:** Conceptualization, Data curation, Formal analysis, Investigation, Methodology, Supervision, Visualization, Writing – original draft, Writing – review & editing. **D. Meyer:** Formal analysis, Investigation, Writing – review & editing. **A. Krivitsky:** Formal analysis, Investigation, Methodology, Validation, Writing – review & editing. **A. R. Studart:** Funding acquisition, Methodology, Resources, Writing – review & editing. **Y. Bao:** Conceptualization, Methodology, Supervision, Writing – original draft, Writing – review & editing. **J.-C. Leroux:** Conceptualization, Funding acquisition, Resources, Supervision, Writing – original draft, Writing – review & editing.

### Data availability

The raw data file is provided as an additional supplementary material.

### Acknowledgements

This project was financed by Swiss National Science Foundation (Sinergia project No. 177178). The authors thank Prof. Kunal Masania (TU Delft) and Dr. Fergal Brian Coulter (ETH Zurich) for designing customized heating system for the DLP printer. We also thank Dr. Kirill Feldman (ETH Zurich) for his help with the tensile testing of our printed samples. Prof. Jan Vermant (ETH Zurich) is acknowledged for providing access to his lab resources.

### References

- Q. Ge, H.J. Qi, M.L. Dunn, Active materials by four-dimension printing, *Appl. Phys. Lett.* 103 (2013), 131901.
- S. Tibbitts, 4D printing: multi-material shape change, *Archit. Des.* 84 (2014) 116–121.
- X. Kuang, et al., Advances in 4D printing: materials and applications, *Adv. Funct. Mater.* 29 (2019) 1805290.
- F. Momeni, M. Mehdi, N.S. Hassani, X. Liu, J. Ni, A review of 4D printing, *Mater. Des.* 122 (2017) 42–79.
- A. Kirillova, et al., Fabrication of biomedical scaffolds using biodegradable polymers, *Chem. Rev.* 121 (2021) 11238–11304.
- A. Lendlein, M. Behl, B. Hiebl, C. Wischke, Shape-memory polymers as a technology platform for biomedical applications, *Expert Rev. Med. Dev.* 7 (2010) 357–379.
- A. Lendlein, S. Kelch, Shape-memory polymers, *Angew. Chem. Int. Ed.* 41 (2002) 2034–2057.
- S. Miao, et al., 4D printing of polymeric materials for tissue and organ regeneration, *Mater. Today* 20 (2017) 577–591.
- M. Behl, A. Lendlein, Shape-memory polymers, *Mater. Today* 10 (2007) 20–28.
- M. Zarek, et al., 3D printing of shape memory polymers for flexible electronic devices, *Adv. Mater.* 28 (2016) 4449–4454.
- H. Yang, et al., 3D printed photoresponsive devices based on shape memory composites, *Adv. Mater.* 29 (2017) 1701627.
- N. Maity, et al., A personalized multifunctional 3D printed shape memory-displaying, drug releasing tracheal stent, *Adv. Funct. Mater.* 31 (2021) 2108436.
- B. Zhang, et al., Self-healing four-dimensional printing with an ultraviolet curable double-network shape memory polymer system, *ACS Appl. Mater. Interfaces* 11 (2019) 10328–10336.
- C. Lin, et al., 4D-printed biodegradable and remotely controllable shape memory occlusion devices, *Adv. Funct. Mater.* 29 (2019) 1906569.
- T.R. Yeazel, M.L. Becker, Advancing toward 3D printing of bioresorbable shape memory polymer stents, *Biomacromolecules* 21 (2020) 3957–3965.
- L. Xue, S. Dai, Z. Li, Biodegradable shape-memory block co-polymers for fast self-expandable stents, *Biomaterials* 31 (2010) 8132–8140.
- D. Jaque, et al., Nanoparticles for photothermal therapies, *Nanoscale* 6 (2014) 9494–9530.
- H. Wei, et al., Direct-write fabrication of 4D active shape-changing structures based on a shape memory polymer and its nanocomposite, *ACS Appl. Mater. Interfaces* 9 (2017) 876–883.
- Y.Y.C. Choong, S. Maleksaeedi, H. Eng, J. Wei, P.-C. Su, 4D printing of high performance shape memory polymer using stereolithography, *Mater. Des.* 126 (2017) 219–225.
- X. Kuang, et al., Grayscale digital light processing 3D printing for highly functionally graded materials, *Sci. Adv.* 5 (2019) eaav5790.
- C. Yu, et al., Photopolymerizable biomaterials and light-based 3D printing strategies for biomedical applications, *Chem. Rev.* 120 (2020) 10695–10743.
- A. Bagheri, J. Jin, Photopolymerization in 3D printing, *ACS Appl. Polym. Mater.* 1 (2019) 593–611.
- A. Andreu, et al., 4D printing materials for vat photopolymerization, *Addit. Manuf.* 44 (2021), 102024.
- Q. Ge, et al., Multimaterial 4D printing with tailorable shape memory polymers, *Sci. Rep.* 6 (2016) 31110.
- Z. Fang, et al., Modular 4D printing via interfacial welding of digital light-controllable dynamic covalent polymer networks, *Matter* 2 (2020) 1187–1197.
- A. Cosola, et al., DLP 3D – printing of shape memory polymers stabilized by thermoreversible hydrogen bonding interactions, *Appl. Mater. Today* 23 (2021), 101060.
- C.A. Spiegel, M. Hackner, V.P. Bothe, J.P. Spatz, E. Blasco, 4D printing of shape memory polymers: from macro to micro, *Adv. Funct. Mater.* 2110580 (2022), <https://doi.org/10.1002/adfm.202110580>.
- B. Zhang, et al., Mechanically robust and UV-curable shape-memory polymers for digital light processing based 4D printing, *Adv. Mater.* 33 (2021) 2101298.
- H. Wu, P. Chen, C. Yan, C. Cai, Y. Shi, Four-dimensional printing of a novel acrylate-based shape memory polymer using digital light processing, *Mater. Des.* 171 (2019), 107704.
- X. Li, et al., Four-dimensional printing of shape memory polyurethanes with high strength and recyclability based on Diels-Alder chemistry, *Polymer* 200 (2020), 122532.
- A. Lendlein, R. Langer, Biodegradable, elastic shape-memory polymers for potential biomedical applications, *Science* 296 (2002) 1673–1676.
- M.C. Serrano, L. Carbajal, G.A. Ameer, Novel biodegradable shape-memory elastomers with drug-releasing capabilities, *Adv. Mater.* 23 (2011) 2211–2215.
- H. Ramaraju, R.E. Akman, D.L. Safranski, S.J. Hollister, Designing biodegradable shape memory polymers for tissue repair, *Adv. Funct. Mater.* 30 (2020) 2002014.
- N. Paunović, et al., Digital light 3D printed bioresorbable and NIR-responsive devices with photothermal and shape-memory functions, *Adv. Sci.* 2200907 (2022), <https://doi.org/10.1002/advs.202200907>.
- M. Zarek, N. Mansour, S. Shapira, D. Cohn, 4D printing of shape memory-based personalized endoluminal medical devices, *Macromol. Rapid Commun.* 38 (2017) 1600628.
- G. Le Fer, M.L. Becker, 4D printing of resorbable complex shape-memory poly(propylene fumarate) star scaffolds, *ACS Appl. Mater. Interfaces* 12 (2020) 22444–22452.
- B.L. Dargaville, et al., Cross-linked poly(trimethylene carbonate-co-L-lactide) as a biodegradable, elastomeric scaffold for vascular engineering applications, *Biomacromolecules* 12 (2011) 3856–3869.
- N. Paunović, et al., Digital light 3D printing of customized bioresorbable airway stents with elastomeric properties, *Sci. Adv.* 7 (2021) abe9499.
- B.G. Amsden, G. Misra, F. Gu, H.M. Younes, Synthesis and characterization of a photo-cross-linked biodegradable elastomer, *Biomacromolecules* 5 (2004) 2479–2486.
- W.F. Hosford, Mechanical Testing. In *Solid Mechanics* 36–37, Cambridge University Press, 2010.
- Y. Wang, et al., 4D multimaterial printing of programmable and selective light-activated shape-memory structures with embedded gold nanoparticles, *Adv. Mater. Technol.* 7 (2021) 2101058.
- A. Czyski, E. Szalek, An HPLC method for levofloxacin determination and its application in biomedical analysis, *J. Anal. Chem.* 71 (2016) 840–843.
- M. Sandmeier, et al., Solvent-free three-dimensional printing of biodegradable elastomers using liquid Macrophotoinitiators, *Macromolecules* 54 (2021) 7830–7839.
- N. Paunović, J.-C. Leroux, Y. Bao, 3D printed elastomers with Sylgard-184-like mechanical properties and tuneable degradability, *Polym. Chem.* 13 (2022) 2271–2276.
- Y. Bao, N. Paunović, J.-C. Leroux, Challenges and opportunities in 3D printing of biodegradable medical devices by emerging photopolymerization techniques, *Adv. Funct. Mater.* 32 (2022) 2109864.
- R.J. Mondschein, A. Kanitkar, C.B. Williams, S.S. Verbridge, T.E. Long, Polymer structure-property requirements for stereolithographic 3D printing of soft tissue engineering scaffolds, *Biomaterials* 140 (2017) 170–188.
- S. Schüller-Ravoo, S.M. Teixeira, J. Feijen, D.W. Grijpma, A.A. Poot, Flexible and elastic scaffolds for cartilage tissue engineering prepared by stereolithography using poly(trimethylene carbonate)-based resins, *Macromol. Biosci.* 13 (2013) 1711–1719.
- F.P.W. Melchels, J. Feijen, D.W. Grijpma, A poly(D,L-lactide) resin for the preparation of tissue engineering scaffolds by stereolithography, *Biomaterials* 30 (2009) 3801–3809.
- L. Elomaa, et al., Preparation of poly( $\epsilon$ -caprolactone)-based tissue engineering scaffolds by stereolithography, *Acta Biomater.* 7 (2011) 3850–3856.
- C.A.P. Joziassie, H. Veenstra, D.W. Grijpma, A.J. Pennings, On the chain stiffness of poly(lactide)s, *Macromol. Chem. Phys.* 197 (1996) 2219–2229.
- K.J. Zhu, R.W. Hendren, K. Jensen, C.G. Pitt, Synthesis, properties, and biodegradation of poly(1,3-trimethylene carbonate), *Macromolecules* 24 (1991) 1736–1740.
- A.P. Pêgo, A.A. Poot, D.W. Grijpma, J. Feijen, Copolymers of trimethylene carbonate and  $\epsilon$ -caprolactone for porous nerve guides: synthesis and properties, *J. Biomater. Sci. Polym. Ed.* 12 (2001) 35–53.
- M. Younes, et al., Re-evaluation of polyvinylpyrrolidone (E 1201) and polyvinylpyrrolidone (E 1202) as food additives and extension of use of polyvinylpyrrolidone (E 1201), *EFSA J.* 18 (2020) 6215.

- [54] L.J. Tan, W. Zhu, K. Zhou, Recent progress on polymer materials for additive manufacturing, *Adv. Funct. Mater.* 30 (2020) 2003062.
- [55] Y. Chen, S. Zhou, Q. Li, Mathematical modeling of degradation for bulk-erosive polymers: applications in tissue engineering scaffolds and drug delivery systems, *Acta Biomater.* 7 (2011) 1140–1149.
- [56] C. Jie, K.J. Zhu, Preparation, characterization and biodegradable characteristics of poly(D,L-lactide-co-1,3-trimethylene carbonate), *Polym. Int.* 42 (1997) 373–379.
- [57] S. Li, Hydrolytic degradation characteristics of aliphatic polyesters derived from lactic and glycolic acids, *J. Biomed. Mater. Res.* 48 (1999) 342–353.
- [58] M.H. Huang, S. Li, M. Vert, Synthesis and degradation of PLA-PCL-PLA triblock copolymer prepared by successive polymerization of  $\epsilon$ -caprolactone and DL-lactide, *Polymer* 45 (2004) 8675–8681.
- [59] G. Schliecker, C. Schmidt, S. Fuchs, T. Kissel, Characterization of a homologous series of D,L-lactic acid oligomers; a mechanistic study on the degradation kinetics in vitro, *Biomaterials* 24 (2003) 3835–3844.
- [60] Z. Ma, Y. Wu, J. Wang, C. Liu, In vitro and in vivo degradation behavior of poly(trimethylene carbonate-co-D,L-lactic acid) copolymer, *Regen. Biomater.* 4 (2017) 207–213.
- [61] J. Hua, et al., Influence of chain microstructure on the hydrolytic degradation of copolymers from 1,3-trimethylene carbonate and L-lactide, *J. Polym. Sci. Part A Polym. Chem.* 47 (2009) 3869–3879.
- [62] O. Vyavahare, D. Ng, S.L. Hsu, Analysis of structural rearrangements of poly(lactic acid) in the presence of water, *J. Phys. Chem. B* 118 (2014) 4185–4193.
- [63] M. Cai, S. Nie, Y. Du, C. Wang, J. Song, Soft elastomers with programmable stiffness as strain-isolating substrates for stretchable electronics, *ACS Appl. Mater. Interfaces* 11 (2019) 14340–14346.
- [64] S.V. Blokhina, A.V. Sharapova, M.V. Ol'khovich, T.V. Volkova, G.L. Perlovich, Solubility, lipophilicity and membrane permeability of some fluoroquinolone antimicrobials, *Eur. J. Pharm. Sci.* 93 (2016) 29–37.
- [65] H. Liu, et al., Improving the oral absorption of nintedanib by a self-microemulsion drug delivery system: preparation and in vitro/in vivo evaluation, *Int. J. Nanomedicine* 14 (2019) 8739–8751.
- [66] A. Ernst, F.J.F. Herth, *Principles and Practice of Interventional Pulmology*, Springer, New York Heidelberg Dordrecht London, 2013.
- [67] A. Lemaire, et al., Outcomes of tracheobronchial stents in patients with malignant airway disease, *Ann. Thorac. Surg.* 80 (2005) 434–438.
- [68] M. Shaikh, G. Kichenadasse, N.R. Choudhury, R. Butler, S. Garg, Non-vascular drug eluting stents as localized controlled drug delivery platform: preclinical and clinical experience, *J. Control. Release* 172 (2013) 105–117.